

The effects of viscosity on the circumplanetary disks

De-Fu Bu¹, Hsien Shang² and Feng Yuan¹

¹ Key Laboratory for Research in Galaxies and Cosmology, Shanghai Astronomical Observatories, Chinese Academy of Sciences, 80 Nandan Road, Shanghai 200030, China. dfbu@shao.ac.cn; fyuan@shao.ac.cn

² Academia Sinica, Institute of Astronomy and Astrophysics, Taipei, Taiwan. Received [] [] []; accepted [] [] []

Abstract The effects of viscosity on the circumplanetary disks residing in the vicinity of protoplanets are investigated through two-dimensional hydrodynamical simulations with the shearing sheet model. We find that viscosity can affect properties of the circumplanetary disk considerably when the mass of the protoplanet is $M_p \lesssim 33M_\oplus$, where M_\oplus is the Earth mass. However, effects of viscosity on the circumplanetary disk are negligibly small when the mass of the protoplanet $M_p \gtrsim 33M_\oplus$. We find that when $M_p \lesssim 33M_\oplus$, viscosity can disrupt the spiral structure of the gas around the planet considerably and make the gas smoothly distributed, which makes the torques exerted on the protoplanet weaker. Thus, viscosity can make the migration speed of a protoplanet lower. After including viscosity, size of the circumplanetary disk can be decreased by a factor of $\gtrsim 20\%$. Viscosity helps to transport gas into the circumplanetary disk from the differentially rotating circumstellar disk. The mass of the circumplanetary disk can be increased by a factor of 50% after viscosity is taken into account when $M_p \lesssim 33M_\oplus$. Effects of viscosity on the formation of planets and satellites are briefly discussed.

Key words: accretion, accretion disks — hydrodynamics — planets and satellites: formation — Solar system: formation

1 INTRODUCTION

Up to date, more than 500 exoplanets have been detected. Most of the exoplanets are gas giant planets, as massive planets are preferentially observed by current detection methods. Thus, it is important to understand the formation process of gas giant planets. According to the core accretion model, a solid core with several M_\oplus , forms first through coagulation of planetesimals in the circumstellar disk. The protoplanet captures a hydrostatic envelope when its mass is less than $M_p \lesssim 10M_\oplus$ (Mizuno 1980; Stevenson 1982; Bodenheimer & Pollack 1986; Pollack et al. 1996; Ikoma, Nakazawa & Emori 2000; Ikoma, Emori & Nakazawa 2001; Hubickyj, Bodenheimer & Lissauer 2005). Ikoma et al. (2000) showed that run-away gas accretion is triggered when the solid core mass exceeds $\simeq 5 - 20M_\oplus$, the protoplanet quickly increases its mass by gas accretion. A gas giant planet acquires almost all of its mass in the run-away gas accretion phase.

Since gas accreting from a differentially rotating circumstellar disk has nonzero angular momentum, a circumplanetary disk can form around the protoplanet (Tanigawa & Watanabe 2002). The circumplanetary disk can influence many aspects of the protoplanet. For example, previously, when calculating the torque on the protoplanet, the contribution of gas inside the whole Roche lobe (or Hill radius) is

neglected. This may be not appropriate. The size of the circumplanetary disk may be smaller than the Roche lobe (as shown in Section 3.2); therefore, when calculating the torque on the protoplanet the gas inside the Roche lobe but beyond the outer boundary of the circumplanetary disk should be taken into account. Also, properties of the circumplanetary disk can determine the evolution of protoplanet and its resulting mass. Finally, satellites form in the vicinity of the protoplanet; studying the properties of the circumplanetary disk helps to investigate the formation process of the satellites.

Gas accretion process onto a protoplanet have been investigated in global simulations by many authors (e.g. Bryden et al. 1999; Kley 1999; Lubow, Seibert & Artymowicz 1999; Kley, D’Angelo & Henning 2001; D’Angelo, Henning & Kley 2002; Bate et al. 2003; D’Angelo, Kley & Henning 2003). However, since the main purpose of these studies was gap formation and planet migration on a large scale, the region in the vicinity of the protoplanet has not been investigated with sufficient resolution. Thus, in their simulations, properties of the circumplanetary disk were not thoroughly explored. The fine structure of the circumplanetary disk has been investigated with shearing sheet models without viscosity (Tanigawa & Watanabe 2002; Machida et al. 2008; Machida 2009; Machida et al. 2010). A question is the mechanism of angular momentum transport in the circumplanetary disk in their models. Gravitational interaction between the protoplanet and gas can produce spiral shocks inside the Roche lobe (or Hill radius) of a protoplanet. Gas flows into the Hill sphere of a protoplanet through the inner and outer Lagrange points. The gas that flows into the Roche lobe from the inner (outer) Lagrange point will undergo a strong shock on the opposite outer (inner) Lagrange side of the Roche lobe, angular momentum is lost through the collision between gas and shocks. The gas spirals inward toward the protoplanet as a result of successive shocks.

Obviously, there should be viscosity in the circumstellar disk, which drives the gas flow in the disk toward the central star. The most promising origin of viscosity in the circumstellar disk should be magnetic turbulence generated by the magnetorotational instability (MRI) (Balbus & Hawley 1991; 1998). Previous work found that despite the ionization rate of a circumstellar disk is low, magnetic field can remain dynamically important, and MRI perturbations can grow under a wide range of fluid conditions and magnetic field strengths (Salmeron & Wardle 2005). Viscosity may play important roles on the properties of the circumplanetary disk. The angular momentum profiles of a circumplanetary disk may be affected significantly by viscosity. Also, viscosity helps to transport gas into the circumplanetary disk from the differentially rotating circumstellar disk, the mass of the circumplanetary disk may be affected by viscosity significantly. Therefore, it is of great importance to study the effects of viscosity on properties of circumplanetary disk.

In this paper, we study the effects of viscosity on circumplanetary disks with the shearing sheet models. We use an anomalous stress tensor to mimic the shear stress originated from magnetohydrodynamic (MHD) turbulence. In Section 2, we describe our models. Results are described in Section 3. We discuss and summarize our results in Section 4.

2 MODEL

2.1 Equations

We confine our models to two-dimensions. We assume that the temperature is constant and that the self-gravity of the disk is negligible. The orbit of the protoplanet is assumed to be circular in the equatorial plane of the circumstellar disk. The protoplanet is not allowed to migrate.

We consider a local region around a protoplanet, using the shearing sheet model (e.g. Goldreich & Lynden-Bell 1965). We take local Cartesian coordinates rotating with the protoplanet with the origin at the protoplanet and the x - and y - axes in the radial and azimuthal direction of the disk, respectively. We solve the equations of hydrodynamics without self-gravity:

$$\frac{\partial \Sigma}{\partial t} + \nabla \cdot (\Sigma \mathbf{v}) = 0 \quad (1)$$

$$\frac{\partial \mathbf{v}}{\partial t} + (\mathbf{v} \cdot \nabla) \mathbf{v} = -\frac{1}{\Sigma} \nabla P - \nabla \Phi - 2\Omega_p \mathbf{e}_z \times \mathbf{v} + \frac{1}{\Sigma} \nabla \cdot \mathbf{T} \quad (2)$$

where Σ is the surface density, \mathbf{v} is the velocity, P is the vertically integrated gas pressure, Φ is the gravitational potential, Ω_p is the Keplerian angular velocity of the protoplanet, \mathbf{e}_z is the unit vector along the rotation axis of the protoplanet, T is the vertically integrated anomalous stress tensor. We adopt an isothermal equation of state,

$$P = \Sigma c_s^2 \quad (3)$$

where c_s is the sound speed. The angular velocity of the protoplanet is given by

$$\Omega_p = \left(\frac{GM_c}{a_p^3} \right)^{1/2} \quad (4)$$

where G , M_c and a_p are gravitational constant, the mass of the central star and the orbital radius of the protoplanet, respectively. The gravitational potential is given by

$$\Phi = -\frac{3}{2}\Omega_p^2 x^2 - \frac{GM_p}{r} \quad (5)$$

where M_p and r are the mass of the protoplanet and the distance from the center of the protoplanet, respectively. The first term is composed of the gravitational potential of the central star and the centrifugal potential. The second term is the gravitational potential of the protoplanet. The Hill radius inside which the protoplanet gravity dominates is defined as

$$R_H = \left(\frac{M_p}{3M_c} \right)^{1/3} a_p \quad (6)$$

Using the Hill radius, we can rewrite equation (4) as

$$\Phi = \Omega_p^2 \left(-\frac{3x^2}{2} - \frac{3R_H^3}{r} \right) \quad (7)$$

We use the stress tensor T to mimic the shear stress, which is in reality magnetic stress associated with magnetohydrodynamics (MHD) turbulence driven by the magnetorotational instability (MRI). We assume that the only non-zero component of the stress tensor T is

$$T_{xy} = \mu \left(\frac{\partial v_y}{\partial x} + \frac{\partial v_x}{\partial y} \right) \quad (8)$$

This is because MRI is driven only by the shear associated with orbital dynamics. In equation (7), $\mu = \Sigma \alpha c_s^2 / \Omega_k$. α , c_s and Ω_k are viscosity coefficient, sound speed and Keplerian angular velocity about the protoplanet, respectively. Previous paper (e.g. Papaloizou, Nelson & Snellgrove 2004) studying the interaction between a protoplanet and magnetized circumstellar disk found that $\alpha \sim 3 \times 10^{-3}$. The maximum α used in this paper is 3×10^{-3} .

In this paper, we normalize length by the scale height of the circumstellar disk $h = c_s / \Omega_p$, time by the inverse of the Keplerian angular velocity of the protoplanet Ω_p^{-1} , and the surface density by the unperturbed surface density of the standard solar nebular model (Hayashi 1981; Hayashi et al. 1985).

2.2 Numerical method

The numerical simulations are performed using the ZEUS-2D code (Stone & Norman 1992a; 1992b). Our initial settings are similar to those of Machida et al. (2008). The gas flow has a constant shear in the x -direction as

$$\mathbf{v}_0 = \left(0, -\frac{3}{2}x \right) \quad (9)$$

Initially, the gas has uniform surface density of the unperturbed disk. In this paper, our standard computational domain is that $|x| \leq 6 (\equiv x_{max})$ and $|y| \leq 12 (\equiv y_{max})$. We adopt logarithmic spacing grids

with the finest resolution ($\Delta x = 0.003$) around the protoplanet. The total number of grids for our standard computational domain is 500×1000 , the resolution is high enough to study the circumplanetary disk in the vicinity of the protoplanet. We inject gas with the linearized Keplerian shear on $y = y_{max}$, ($0 < x < x_{max}$) and $y = -y_{max}$, ($-x_{max} < x < 0$). For the rest of the boundaries, we adopt outflow boundary conditions.

In order to avoid singularity in the proximity of the protoplanet, the gravitational potential of the protoplanet is smoothed in its neighborhood with

$$\Phi_p = -\frac{GM_p}{(r^2 + r_{sm}^2)^{1/2}} \quad (10)$$

where r_{sm} is the smoothing length of the protoplanet's potential. In this paper, we choose $r_{sm} = 0.05$. Tanigawa & Watanabe (2002) showed that $r_{sm} = 0.05$ is safe to study the properties of the circumplanetary disk in the vicinity of the protoplanet.

In the run-away gas accretion phase, accretion by planet is non-negligible. There should be accretion, neglecting accretion is unphysical. Therefore, we should mimic the accretion process by planet. Because the growth timescale of a planet is much longer than the typical time of our simulations, we should have a constant accretion rate which is independent from the parameters used to mimic the accretion process. As done by Tanigawa & Watanabe (2002), the gas inside r_{sink} is removed by a constant rate $[\Sigma^{n+1} = \Sigma^n(1 - \Delta t)]$, $\Delta t (\ll 1)$ is a time step of the calculations, and superscript n is the number of numerical time step. Tanigawa & Watanabe (2002) have tested the effects of r_{sm} and r_{sink} on the accretion rate of the planet. They found that the results do not depend on the values of r_{sm} and r_{sink} as long as $r_{sm} = r_{sink} < 0.07$. In this paper, we set $r_{sm} = r_{sink} = 0.05$.

2.3 scaling

In the standard solar nebular model (Hayashi 1981; Hayashi et al. 1985), the temperature T , sound speed c_s , and gas density ρ_0 are given by

$$T = 280 \left(\frac{L}{L_\odot} \right)^{1/4} \left(\frac{a_p}{1AU} \right)^{-1/2} \quad (11)$$

where L and L_\odot are the protostellar and solar luminosities;

$$c_s = \left(\frac{kT}{\mu m_H} \right)^{1/2} = 1.9 \times 10^4 \left(\frac{T}{10K} \right)^{1/2} \left(\frac{2.34}{\mu} \right)^{1/2} \text{ cm/s} \quad (12)$$

where $\mu = 2.34$ is the mean molecular weight of the gas composed mainly of H_2 and He ; and

$$\rho_0 = 1.4 \times 10^{-9} \left(\frac{a_p}{1AU} \right)^{-11/4} \text{ g/cm}^3, \quad (13)$$

respectively. When the values of $M_c = 1M_\odot$ and $L = 1L_\odot$ are adopted, using equations (4), (11) and (12), we can describe the scale height h as

$$h = 5.0 \times 10^{11} \left(\frac{a_p}{1AU} \right)^{5/4} \text{ cm}. \quad (14)$$

The mass of the planet in unit of Jupiter mass can be described as

$$\frac{M_p}{M_{Jup}} = 0.12 \left(\frac{M_c}{1M_\odot} \right)^{-1/2} \left(\frac{a_p}{1AU} \right)^{3/4} \left(\frac{R_H}{h} \right)^3 \quad (15)$$

In this paper, we assume that $M_c = 1M_\odot$, $L = 1L_\odot$. The planet is located at $a_p = 5.2AU$. Therefore, the temperature of the gas is $T = 123K$. Because our shearing box just represent a local region around the planet, we further assume that the temperature is uniform in the whole computational domain.

In the paper below, the Hill radius R_H is in unit of h . In table 2, $R_H = 0.4, 0.5$ and 0.63 correspond to planet mass of $0.026, 0.05$ and 0.1 Jupiter mass, respectively.

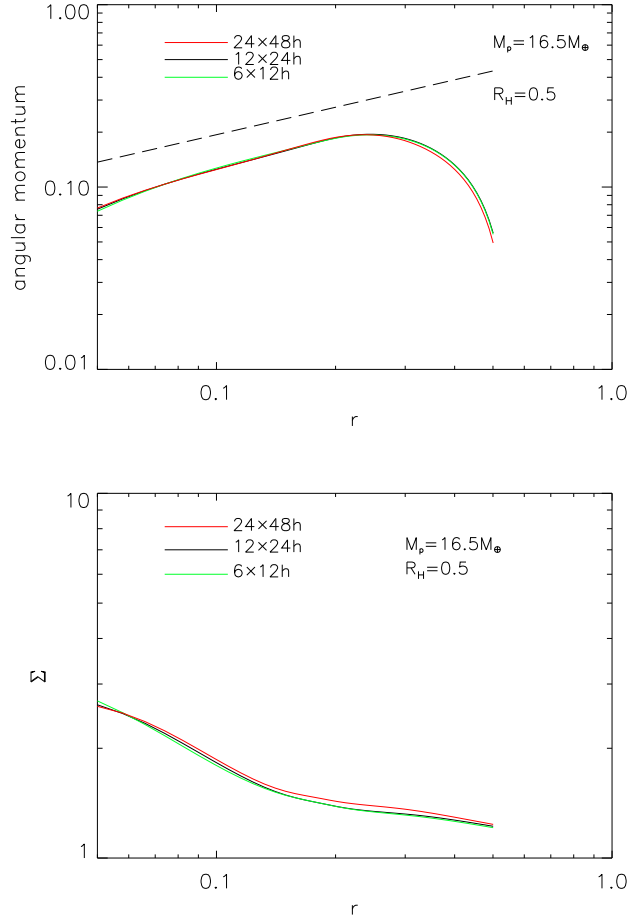


Fig. 1 Specific angular momentum (upper-panel) and surface density (lower-panel) of the circumplanetary disks for a $16.5M_{\oplus}$ protoplanet as a function of distance r from the protoplanet with different sheet size. It can be seen that the effects of sheet size on the structure of the circumplanetary disk are negligible as long as the sheet size is much larger than the Hill radius.

Table 1 Parameters for the test models

Models	Sheet size	Grids	R_H	α
M005V0	$12 \times 24h$	500×1000	0.5	0
BM005V0	$24 \times 48h$	656×1312	0.5	0
SM005V0	$6 \times 12h$	358×716	0.5	0

2.4 Tests of the effects of sheet size on the results

In this section, we study the effects of sheet size on the structure of the circumplanetary disk inside the Hill radius. We find that the flow structure inside the Hill sphere (or circumplanetary disk) does not

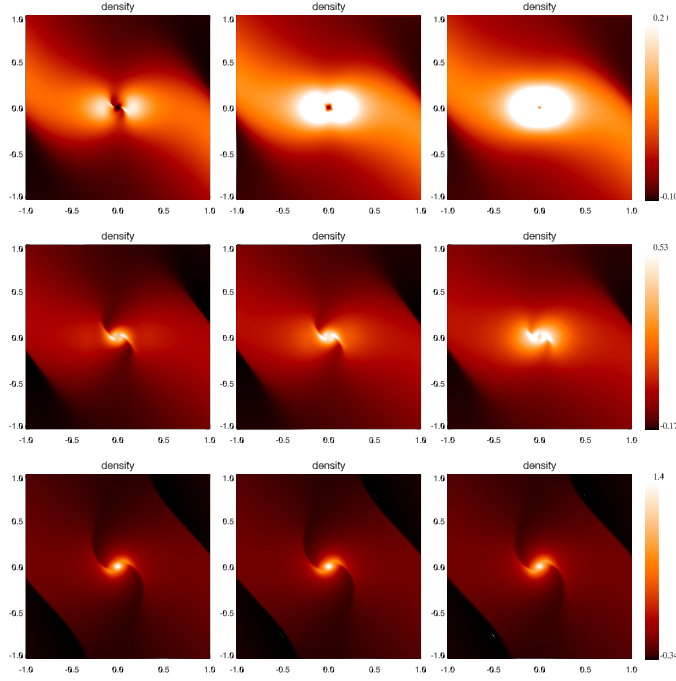


Fig. 2 Contours of logarithm surface density of the circumplanetary disks surrounding protoplanets with mass of 8.5 , 16.5 and $33M_{\oplus}$ (top to bottom rows). The top row panels show the circumplanetary disks surrounding a $8.5M_{\oplus}$ planet. In the top row, the left-, middle- and right-hand panels correspond to models M0026V0 ($\alpha = 0$), M0026V1 ($\alpha = 10^{-3}$) and M0026V2 ($\alpha = 3 \times 10^{-3}$), respectively. The middle row panels show the circumplanetary disks surrounding a $16.5M_{\oplus}$ planet. In the middle row, the left-, middle- and right-hand panels correspond to models M005V0 ($\alpha = 0$), M005V1 ($\alpha = 10^{-3}$) and M005V2 ($\alpha = 3 \times 10^{-3}$), respectively. The bottom row panels show the circumplanetary disks surrounding a $33M_{\oplus}$ planet. In the bottom row, the left-, middle- and right-hand panels correspond to models M01V0 ($\alpha = 0$), M01V1 ($\alpha = 10^{-3}$) and M01V2 ($\alpha = 3 \times 10^{-3}$), respectively.

depend on the computational box size as long as the size is much larger than the Hill radius. Here we just take $R_H = 0.5$, $\alpha = 0$ as a example. Table 1 lists the parameters of the $R_H = 0.5$ tests.

Fig.1 shows the specific angular momentum (upper-panel) and surface density (lower-panel) distribution of the circumplanetary disks for a $16.5M_{\oplus}$ protoplanet with different sheet size. From this figure, we can see that the effects of sheet size on the structure of the circumplanetary disk are negligible as long as the sheet size is much larger than the Hill radius. The results shown in Section 3 is calculated with our standard sheet size $12 \times 24h$.

Table 2 Parameters for all of our models

Models	R_H	M_p	α
M0026V0	0.4	$8.5M_\oplus$	0
M0026V1	0.4	$8.5M_\oplus$	10^{-3}
M0026V2	0.4	$8.5M_\oplus$	3×10^{-3}
M005V0	0.5	$16.5M_\oplus$	0
M005V1	0.5	$16.5M_\oplus$	10^{-3}
M005V2	0.5	$16.5M_\oplus$	3×10^{-3}
M01V0	0.63	$33M_\oplus$	0
M01V1	0.63	$33M_\oplus$	10^{-3}
M01V2	0.63	$33M_\oplus$	3×10^{-3}

3 RESULTS

Table 2 lists all of the models in this paper. We find that all of the models have settled into their steady state before 20 orbits, so that the results shown below at $t = 75$ orbits are fully relaxed.

In order to investigate the effects of viscosity on the circumplanetary disk, for each protoplanet with different mass, we carry out three simulations with different viscosity coefficient α . We find that when the protoplanet mass $M_p \gtrsim 33M_\oplus$, the effects of viscosity are negligible.

3.1 Circumplanetary disk structure and migration of protoplanets

Fig.2 shows the circumplanetary disks structure around protoplanets with mass of 8.5, 16.5 and $33M_\oplus$ (top to bottom rows). The top row panels show the circumplanetary disks surrounding a $8.5M_\oplus$ protoplanet. In the top row, the left-, middle- and right-hand panels correspond to models M0026V0 ($\alpha = 0$), M0026V1 ($\alpha = 10^{-3}$) and M0026V2 ($\alpha = 3 \times 10^{-3}$), respectively. The middle row panels show the circumplanetary disks surrounding a $16.5M_\oplus$ protoplanet. In the middle row, the left-, middle- and right-hand panels correspond to models M005V0 ($\alpha = 0$), M005V1 ($\alpha = 10^{-3}$) and M005V2 ($\alpha = 3 \times 10^{-3}$), respectively. The bottom row panels show the circumplanetary disks surrounding a $33M_\oplus$ protoplanet. In the bottom row, the left-, middle- and right-hand panels correspond to models M01V0 ($\alpha = 0$), M01V1 ($\alpha = 10^{-3}$) and M01V2 ($\alpha = 3 \times 10^{-3}$), respectively. It can be seen clearly that as the mass of the protoplanet increases, the spiral structure of the circumplanetary disk becomes more prominent, higher mass protoplanet can excite higher amplitude spiral shock.

For the protoplanet with mass of $8.5M_\oplus$, with the increase of strength of viscosity, the spiral structure is getting weaker. The spiral structure completely disappears when $\alpha = 3 \times 10^{-3}$ and the circumplanetary disk is nearly axisymmetric about the protoplanet. For a $8.5M_\oplus$ protoplanet, the maximum surface density of the spiral waves is only 2 times bigger than the minimum surface density; the amplitude of the spiral wave is weak, viscosity can easily disrupt the spiral structure and make the gas in the circumplanetary disk smoothly distributed. For the protoplanet with mass of $16.5M_\oplus$, viscosity also makes the spiral structure of the circumplanetary disk weaker. But the effect is small compared to the smaller protoplanet mass case ($M_p = 8.5M_\oplus$). This is because with the increase of the mass of the protoplanet, the amplitude of the spiral waves gets higher, viscosity can hardly affect the spiral structure. It can be seen that when the protoplanet mass reaches $33M_\oplus$, viscosity almost plays no roles on the circumplanetary disk structure.

The protoplanet excites spiral density waves at the Lindblad resonance and the torques exerted on the protoplanet as the reaction of exciting waves make the orbit of the protoplanet around central star change. Previous works (Lubow et al. 1999; Tanigawa & Watanabe 2002) found that the spiral structure around the protoplanet can affect the torques significantly. In the limiting case, if the gas distribution around a protoplanet is perfectly axisymmetric about the protoplanet, the torques exerted on the protoplanet will be zero. From Fig.2, we find that viscosity can disrupt the spiral structure considerably when the mass of protoplanet $M_p \lesssim 33M_\oplus$. Thus, we can expect that when the protoplanet is small ($M_p \lesssim 33M_\oplus$), viscosity can affect the torques exerted on the protoplanet considerably.

It is always believed that the gas inside the Hill sphere of a planet migrates with the planet. Therefore, in most previous works, when calculating the torque exerted on a planet, the contribution from the gas inside the Hill sphere is completely excluded. However, Crida et al. (2009) showed that the gas bound to the planet (circumplanetary disk) only exists inside $0.5R_H$. In the region $0.5R_H < r < R_H$, the gas is not bound to the planet. Therefore, when calculating the torque, the gas inside the Hill sphere should not be excluded completely.

Now, we quantitatively study the effects of viscosity on the torques exerted on a protoplanet. Since we adopt the local approximation, the net torque in our simulation becomes exactly zero. But an actual net torque is not zero, owing to slight asymmetry of density distribution, temperature and the curvature of the protoplanet orbit. The net torque exerted on the protoplanet is roughly proportional to the one-side torque exerted by the gas exterior to the orbit of the protoplanet (Tanigawa & Watanbe 2002)¹; therefore, the one-side torque would be a clue to solve the migration problem. Because we adopt the local approximation, we just discuss the effects of viscosity on the one-side 'force' exerted on the protoplanet. The 'force' corresponds to the torque divided by the semimajor axis of the protoplanet. The one-side force exerted on a protoplanet is defined by

$$F_{y,out}(r_{mask}) = \int_0^{x_{max}} \int_{-y_{max}}^{y_{max}} \Sigma \frac{\partial \Phi}{\partial y} \theta(r - r_{mask}) dy dx \quad (16)$$

where r_{mask} is the artificial inner limit of the force integration, and θ is the step function. If $r > r_{mask}$, $\theta = 1$, otherwise $\theta = 0$. The 'force density' is defined as $dF(x) = \int_{-y_{max}}^{y_{max}} \Sigma \frac{\partial \Phi}{\partial y} dy$.

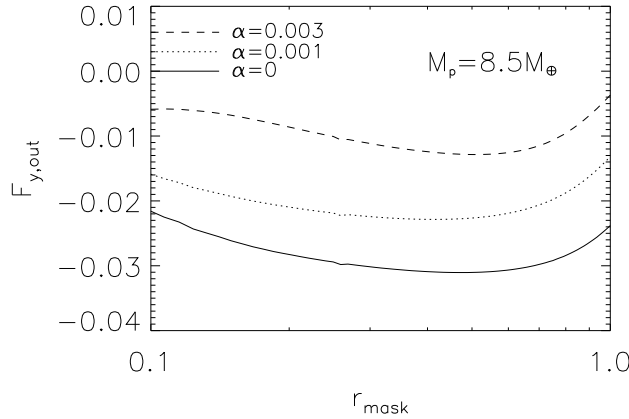


Fig. 3 Gravitational force exerted on the $8.5M_{\oplus}$ protoplanet from disk gas in $x > 0$ as a function of r_{mask} , within which gas is excluded from force integration. In this figure, the solid, dotted and dashed lines correspond to models M0026V0 ($\alpha = 0$), M0026V1 ($\alpha = 10^{-3}$) and M0026V2 ($\alpha = 3 \times 10^{-3}$), respectively.

We show $F_{y,out}$ as a function of r_{mask} for a protoplanet with mass of $8.5M_{\oplus}$ in Fig.3. In Section 3.2, we show that the outer boundary of $8.5M_{\oplus}$ and $16.5M_{\oplus}$ protoplanets located inside $r = 0.22$, therefore we can focus on the torque exerted by the gas beyond $r = 0.22$. The gas in $x > 0$ exerts a

¹ Net torque is the difference of the two opposite-signed one-side torques, and the ratio of the two one-side torques does not change very much when one change parameters such as planet mass or temperature in linear regime. Thus, at least in this regime, we can say that the net torque is proportional to one-side torque.

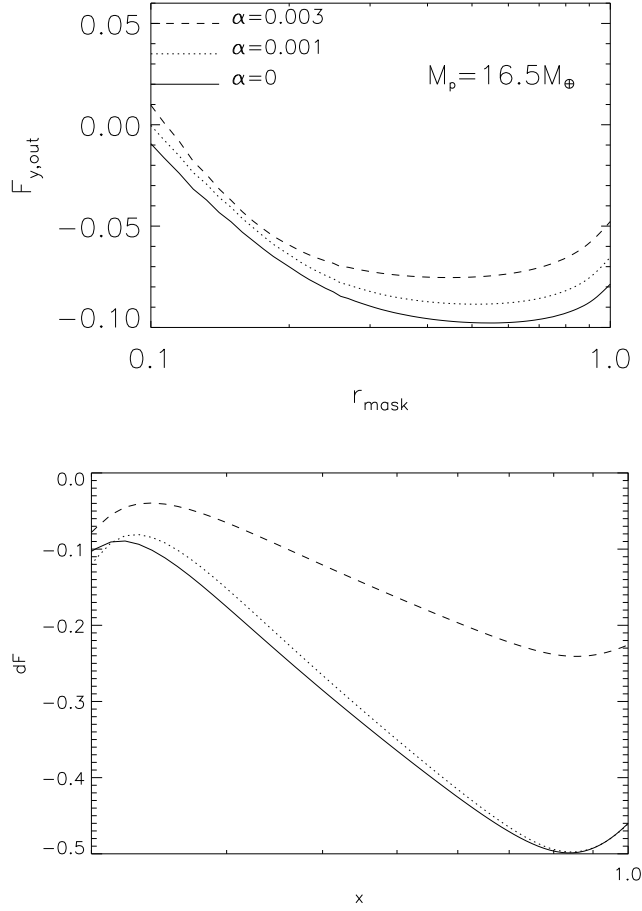


Fig. 4 Upper-panel shows the gravitational force exerted on the $16.5M_{\oplus}$ protoplanet from disk gas in $x > 0$ as a function of r_{mask} , within which gas is excluded from force integration. In this panel, the solid, dotted and dashed lines correspond to models M005V0 ($\alpha = 0$), M005V1 ($\alpha = 10^{-3}$) and M005V2 ($\alpha = 3 \times 10^{-3}$), respectively. Lower-panel shows the torque density as a function of distance from the $16.5M_{\oplus}$ protoplanet. In this panel, the solid, dotted and dashed lines correspond to models M005V0 ($\alpha = 0$), M005V1 ($\alpha = 10^{-3}$) and M005V2 ($\alpha = 3 \times 10^{-3}$), respectively.

negative torque on the protoplanet, which pushes the protoplanet migrating towards the central star. As expected, when the spiral structure around the planet gets weaker, the force exerted on the protoplanet is decreased significantly. Fig.4 (upper-panel) plots $F_{y,out}$ as a function of r_{mask} for a protoplanet with mass of $16.5M_{\oplus}$. When $\alpha = 3 \times 10^{-3}$, the spiral structure is partially disrupted by viscosity, which also leads to the reduction of the torque exerted on the planet. In order to show clearly the 'torque' is affected by viscosity, the lower panel of Fig.4 plots the 'torque density' as a function of distance from the planet. The case for a $8.5M_{\oplus}$ protoplanet is similar. We find when $M_p \geq 33M_{\oplus}$, the effect of viscosity on

the torque exerted on protoplanets is negligible. We conclude that the viscosity can affect the torques exerted on a protoplanets considerably by disrupting the spiral structure of gas disk when the mass of the protoplanet is small ($M_p \lesssim 33M_\oplus$).

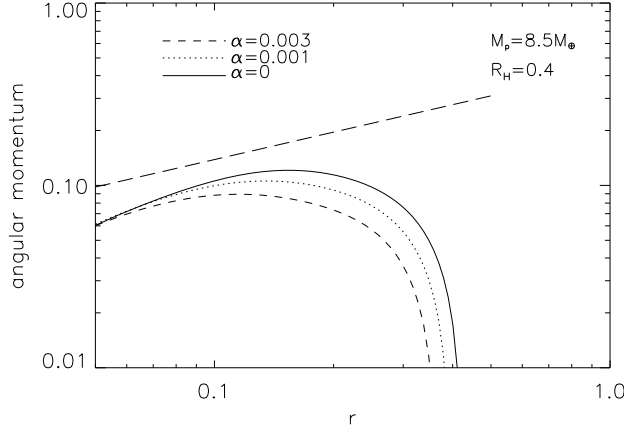


Fig. 5 Specific angular momentum of the circumplanetary disks surrounding a $8.5M_\oplus$ protoplanet. In this figure, the solid, dotted and dashed lines correspond to models M0026V0 ($\alpha = 0$), M0026V1 ($\alpha = 10^{-3}$) and M0026V2 ($\alpha = 3 \times 10^{-3}$), respectively. The long-dashed line corresponds to the Keplerian angular momentum with respect to the protoplanet.

3.2 Circumplanetary disk size

Now, we investigate the effects of viscosity on the size of the circumplanetary disks. The radial edge of a circumplanetary disk is taken as the point of turnover in the specific angular momentum of the disk. Quillen & Trilling (1998) made a simple analytic prediction of the approximate circumplanetary disk radii around accreting protoplanets. They assume that the gas flows into the Hill sphere of a protoplanet via the inner and outer Lagrange points. They also assume that when the gas arrives at the Lagrange points, the velocity, relative to the Lagrange points, is negligibly small. The Lagrange points have the same angular velocity around the central star as the protoplanet. The Lagrange points are approximately located at

$$r = a_p \pm R_H \quad (17)$$

Thus, when the gas at the Lagrange points is captured by the protoplanet, its specific angular momentum relative to the protoplanet is

$$j \simeq R_H^2 \Omega_p \quad (18)$$

Assuming conservation of angular momentum when the accreting gas flows towards the protoplanet, the centrifugal radius, r_c , of the circumplanetary disk is

$$\frac{j^2}{r_c^2} \approx \frac{GM_p}{r_c} \quad (19)$$

which yields

$$r_c \approx R_H/3. \quad (20)$$

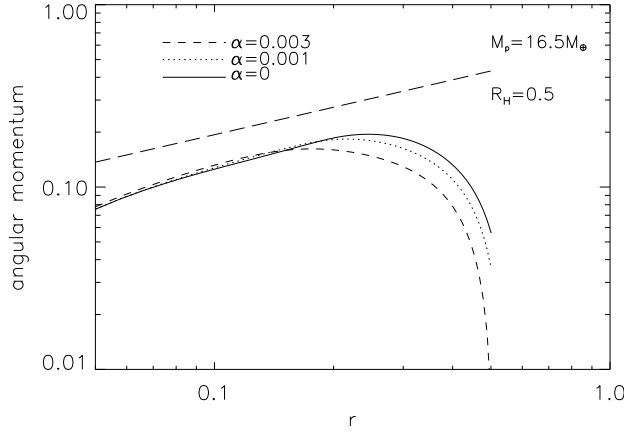


Fig. 6 Specific angular momentum of the circumplanetary disks surrounding a $16.5M_{\oplus}$ protoplanet. In this figure, the solid, dotted and dashed lines correspond to models M005V0 ($\alpha = 0$), M005V1 ($\alpha = 10^{-3}$) and M005V2 ($\alpha = 3 \times 10^{-3}$), respectively. The long-dashed line corresponds to the Keplerian angular momentum with respect to the protoplanet.

Thus, the typical size of a circumplanetary disk should be approximate $R_H/3$.

Fig. 5 shows the specific angular momentum of the circumplanetary disks around a $8.5M_{\oplus}$ protoplanet. In this figure, the solid, dotted and dashed lines correspond to models M0026V0 ($\alpha = 0$), M0026V1 ($\alpha = 10^{-3}$) and M0026V2 ($\alpha = 3 \times 10^{-3}$), respectively. We can see the outer boundary of a non-viscous circumplanetary disk (model M0026V0) around a $8.5M_{\oplus}$ protoplanet locates at $r = 0.15$, the disk size does not differ greatly from the $R_H/3$ prediction. Beyond $r = 0.15$, the gas rotates around the central star, the angular momentum becomes smaller and smaller with increasing distance from the protoplanet. The angular momentum relative to the protoplanet even becomes negative when the distance from the protoplanet is sufficiently big which is not shown in Fig. 5. When viscosity is included, the size of the circumplanetary disk decreases. In model M0026V2, the outer boundary of the circumplanetary disk locates at $r = 0.11$, the size of the disk is reduced by a factor of 27% compared to the non-viscous disk. As can be seen from Fig. 5, the specific angular momentum of the circumplanetary disk becomes lower after including viscosity, which is due to the outward angular momentum transfer by viscosity. The variation of angular momentum at given radius is determined by the divergence of the viscous stress; at the outer boundary of the circumplanetary disk, the divergence of viscosity is stronger than that at other radii due to the stronger shear of the gas (it can be clearly seen from Fig. 5), which makes the decreasing amplitude of the angular momentum at the outer boundary much larger than that of the gas at other radii. Therefore, the outer boundary of the circumplanetary disk is moved inward when viscosity is taken into account.

Fig. 6 shows the specific angular momentum of the circumplanetary disks around a $16.5M_{\oplus}$ protoplanet. In this figure, the solid, dotted and dashed lines correspond to models M005V0 ($\alpha = 0$), M005V1 ($\alpha = 10^{-3}$) and M005V2 ($\alpha = 3 \times 10^{-3}$), respectively. The outer boundary of the circumplanetary disk is also moved inward when viscosity is included. The outer boundary of a non-viscous circumplanetary disk (model M005V0) around a $16.5M_{\oplus}$ protoplanet locates at $r = 0.22$. In model M005V2, the outer boundary of the circumplanetary disk locates at $r = 0.17$, the size of the disk is reduced by a factor of 23% compared to the non-viscous disk. We find that when the protoplanet mass $M_p \gtrsim 33M_{\oplus}$, the effect of viscosity on the size of a circumplanetary disk is negligibly small.

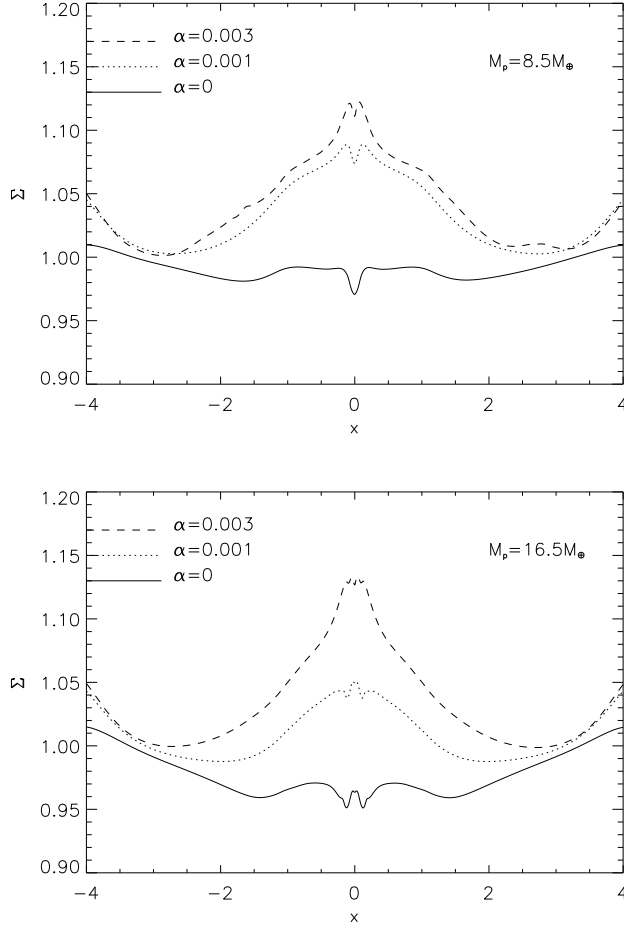


Fig. 7 The surface density averaged over y against x for the gas around protoplanets. The upper and lower panels correspond to 8.5 and $16.5 M_{\oplus}$ protoplanets, respectively. In the upper panel, the solid, dotted and dashed lines correspond to models M0026V0 ($\alpha = 0$), M0026V1 ($\alpha = 10^{-3}$) and M0026V2 ($\alpha = 3 \times 10^{-3}$), respectively. In the lower panel, the solid, dotted and dashed lines correspond to models M005V0 ($\alpha = 0$), M005V1 ($\alpha = 10^{-3}$) and M005V2 ($\alpha = 3 \times 10^{-3}$), respectively.

Crida et al. (2009) have found that the size of the circumplanetary disk $\sim 0.5 R_H$, which is slightly larger than that obtained in this paper. This is because Crida use a energy equation to solve internal energy of the gas. With the energy equation, the collapse of the gas onto the circumplanetary disk is limited by the heating due to adiabatic compression, which gives a wider circumplanetary disk than in the locally isothermal case.

From Fig. 5 and Fig. 6, we see that the rotational velocity of the disk around the planets is significantly sub-Keplerian. The reason is as follows. In the radial direction, gravitational force is balanced by centrifugal force and pressure gradient force. If the temperature of the gas is fixed, with the increasing

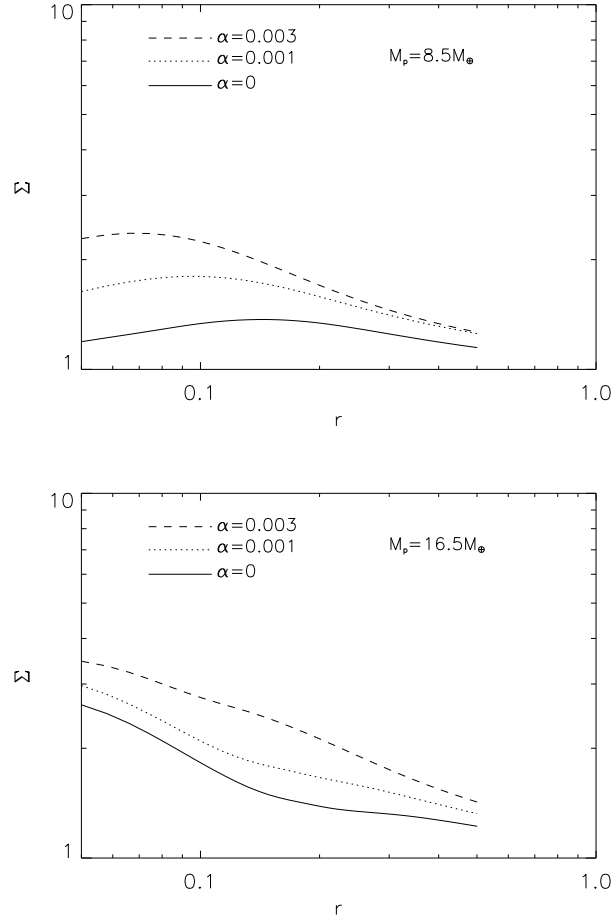


Fig. 8 Surface density of the circumplanetary disks as a function of distance r from the protoplanet. The upper and lower panels correspond to 8.5 and $16.5 M_{\oplus}$ protoplanets, respectively. In the upper panel, the solid, dotted and dashed lines correspond to models M0026V0 ($\alpha = 0$), M0026V1 ($\alpha = 10^{-3}$) and M0026V2 ($\alpha = 3 \times 10^{-3}$), respectively. In the lower panel, the solid, dotted and dashed lines correspond to models M005V0 ($\alpha = 0$), M005V1 ($\alpha = 10^{-3}$) and M005V2 ($\alpha = 3 \times 10^{-3}$), respectively.

of planet mass, the centrifugal force will increase (rotational velocity increase). In our paper, the mass of the planet is small (around 10 earth mass), so pressure gradient force is important, the gas rotates sub-keplerian. Tanigawa, Ohtsuki & Machida (2012) found that the gas around the planet rotates almost Keplerian. The reason is as follows. In Tanigawa, Ohtsuki & Machida, ApJ (2012), the temperature is identical to that in our paper, but their planet mass is 1 Jupiter mass which is much bigger than the planet mass in our paper. Therefore, in Tanigawa, Ohtsuki & Machida (2012), the gas rotates almost keplerian.

3.3 Circumplanetary disk mass

In the standard picture, a protoplanet residing in a circumstellar disk can exert torques on the circumstellar disk through the excitation of spiral density waves (e.g. Goldreich & Tremaine 1979). The angular momentum carried by the density waves will be deposited in the circumstellar disk where the waves are damped. The circumstellar disk gas exterior to the protoplanet orbit gets positive angular momentum and thus moves outward. The circumstellar disk gas interior to the protoplanet orbit gets negative angular momentum and thus moves inward. For a low-mass protoplanet, a partial density gap forms along the orbit of the protoplanet. However, the viscosity inside the circumstellar disk tries to transport gas into the low density partial gap region, which makes the density gap less prominent. Viscosity can affect the depth of the density gap around the orbit of the protoplanet and thus affects the circumplanetary disk mass.

In Fig. 7, we plot the surface density averaged over y against x for the gas around protoplanets. The upper and lower panels correspond to 8.5 and $16.5M_{\oplus}$ protoplanets, respectively. In the upper panel, the solid, dotted and dashed lines correspond to models M0026V0 ($\alpha = 0$), M0026V1 ($\alpha = 10^{-3}$) and M0026V2 ($\alpha = 3 \times 10^{-3}$), respectively. In the lower panel, the solid, dotted and dashed lines correspond to models M005V0 ($\alpha = 0$), M005V1 ($\alpha = 10^{-3}$) and M005V2 ($\alpha = 3 \times 10^{-3}$), respectively. It is obviously seen that the protoplanets try to open a density gap along its orbit. As expected, the protoplanet in the inviscid gas produces a deeper and wider gap than others.

In Fig. 8, we plot the surface density profiles of the circumplanetary disks around protoplanets. The upper and lower panels correspond to 8.5 and $16.5M_{\oplus}$ protoplanets, respectively. In the upper panel, the solid, dotted and dashed lines correspond to models M0026V0 ($\alpha = 0$), M0026V1 ($\alpha = 10^{-3}$) and M0026V2 ($\alpha = 3 \times 10^{-3}$), respectively. In the lower panel, the solid, dotted and dashed lines correspond to models M005V0 ($\alpha = 0$), M005V1 ($\alpha = 10^{-3}$) and M005V2 ($\alpha = 3 \times 10^{-3}$), respectively. Viscosity makes it easier for gas flows towards the protoplanet. Therefore, the surface density of the circumplanetary disk in the viscous gas is higher than that of the inviscid gas. We have calculated the circumplanetary disk mass. For a $8.5M_{\oplus}$ protoplanet, when $\alpha = 3 \times 10^{-3}$, the disk mass is bigger than the inviscid disk by a factor of 56%. For a $16.5M_{\oplus}$ protoplanet, when $\alpha = 3 \times 10^{-3}$, the disk mass is bigger than the inviscid disk by an alternative factor of 50%. We find that when $M_p \gtrsim 33M_{\oplus}$, the effect of viscosity on circumplanetary disk mass is negligibly small.

3.4 Mass accretion rate

We talk about the mass accretion rate in this section. We talk about mass accretion rate in real unit (equations (11)-(15)). We assume that the planets locate at $a_p = 5.2AU$. Also, we assume that $M_c = 1M_{\odot}$ and $L = 1L_{\odot}$. In this paper, we find that the mass accretion rates for non-viscous models M0026V0 ($8.5M_{\oplus}$) and M005V0 ($16.5M_{\oplus}$) are $2.2 \times 10^{-5}M_{Jup}/yr$ and $5.0 \times 10^{-5}M_{Jup}/yr$, respectively. Almost all of the numerical settings of Tanigawa & Watanabe (2002) are same as that in this paper. The only difference is that their is no viscosity in Tanigawa & Watanabe (2002). In Tanigawa & Watanabe (2002), the smallest mass used is $22M_{\oplus}$. Therefore, we can not directly compare our result to theirs. Fortunately, in equation (19) in Tanigawa & Watanabe (2002), they give the dependence of mass accretion rate on the planet mass. Using their equation (19), the mass accretion rate for $8.5M_{\oplus}$ and $16.5M_{\oplus}$ are $2.02 \times 10^{-5}M_{Jup}/yr$ and $4.8 \times 10^{-5}M_{Jup}/yr$, respectively. Our results for non-viscous gas are consistent with that in Tanigawa & Watanabe (2002).

If viscosity is included, we find that the mass accretion rate becomes higher. The mass accretion rate for the viscous models M0026V2 ($8.5M_{\oplus}$ and $\alpha = 3 \times 10^{-3}$) and M005V2 ($16.5M_{\oplus}$ and $\alpha = 3 \times 10^{-3}$) are $4 \times 10^{-5}M_{Jup}/yr$ and $8.0 \times 10^{-5}M_{Jup}/yr$, respectively. D'Angelo et al. (2002) using global simulations to study the gas flow onto planets. For a $6.4M_{\oplus}$ planet, when $\alpha = 4 \times 10^{-3}$, they find that the mass accretion rate is $1.2 \times 10^{-5}M_{Jup}/yr$ (Fig. 25 in their papers). For a $15M_{\oplus}$ planet, when $\alpha = 4 \times 10^{-3}$, they find that the mass accretion rate is $1.5 \times 10^{-5}M_{Jup}/yr$ (Fig. 25 in their papers). Given that the viscosity and planet mass are comparable, it seems that the accretion rate found in this paper is much higher than that obtained in D' Angelo et al. (2002). The reason may be due to the

depletion of the gas inside the orbital radius of the planet in the global simulations in D' Angelo et al. (2002).

The Bondi accretion rates for $8.5M_{\oplus}$ and $16.5M_{\oplus}$ planets located at $5.2AU$ are $1 \times 10^{-4}M_{Jup}/yr$ and $3.8 \times 10^{-4}M_{Jup}/yr$, respectively. The angular momentum of the gas makes the actual accretion rate much smaller than the Bondi accretion rate of the planets. We must note that the mass accretion rate obtained in this paper may be not accurate. This is because, inside the Hill radius, the gas may evolve adiabatically, the increased temperature towards the planet may make accretion rates smaller than that obtained in this paper.

4 SUMMARY AND DISCUSSION

We investigate the effects of viscosity on the circumplanetary disks forming in the vicinity of the protoplanet through two-dimensional hydrodynamical simulations with the shearing sheet model. We find that viscosity can affect the properties of the circumplanetary disk significantly when the mass of the protoplanet $M_p \lesssim 33M_{\oplus}$.

Local shearing-sheet approximation is only an approximation of the global model, and it may not be appropriate for investigating the global evolution of the disk structure. However, Muto et al. (2010) have shown that the local shearing-sheet approximation and full global model share many essential physics in common. Muto et al. (2010) have also shown that the one-dimensional disk evolution model constructed from the global model and the local model are very similar. Therefore we expect the local simulations have captured the main physics of the circumplanetary disks.

Physically we should use three-dimensional simulations to study the circumplanetary disks inside the Hill radius. However, as a first step, we carry out these simulations in order to understand the basic effects of viscosity on the circumplanetary disks. The two-dimensional simulations can capture the main physics of the disks. For example, the mass accretion rate can be generated properly by two-dimensional simulations because the accretion rate is determined mainly by the flow where $r > R_H$ (when $r > R_H$, the disk is very thin and two-dimensional simulations is enough) (Tanigawa & Watanabe 2002). Although the 2D simulations can capture some properties of the circumplanetary disk, some important feature may lost in the 2D disks. For example, Tanigawa, Ohtsuki & Machida (2012) found that most of gas accretion onto circumplanetary disks occurs nearly vertically toward the disk surface from high altitude, which can not be found in 2D simulations. In a subsequent paper, we will discuss the effects of viscosity on the circumplanetary disks in three-dimensions.

In this paper, we use a smoothing length to smooth the gravity close to the planet. Muller (et al. 2012) find that for longer distances, the smooth length is determined solely by the vertical disk thickness. For the planet case they find that outside $r = H$, when the value of $r_{sm} = 0.7H$ describes the averaged force very well. However, for shorter distances the smoothing needs to be reduced significantly. In this paper, in order to study the structure of circumplanetary disks we adopt $r_{sm} = 0.05H$. This value is proved to be safe to study the circumplanetary disks by Tanigawa & Watanabe (2002).

In this paper, we just use an anomalous stress tensor to mimic the shear stress, which is in reality magnetic stress associated with magnetohydrodynamic (MHD) turbulence driven by the magnetorotational instability (MRI). In a real turbulent circumplanetary disk, the properties of the disk should fluctuate with time, but we expect that the time-averaged properties of the turbulent disk should be consistent with our results here. The spiral shocks in the circumplanetary disk also can affect the amplitude of the turbulent stress, but the effect is small when the mass of the protoplanet is small ($M_p \lesssim 30M_{\oplus}$) (Papaloizou et al. 2004). Thus, our calculations have captured the main physics of the circumplanetary disk.

To properly study the viscous circumplanetary disk, it is necessary to include magnetic effects. However, the gas in the circumstellar disk surrounding a protostar is just weakly ionized. Weakly ionized plasma is subject to a number of non-idea MHD effects due to the collisional coupling between the ionized species and the neutrals (e.g. ambipolar diffusion effects) (Bai & Stone 2011). The magnetorotational instability (MRI), which is considered as the major mechanism for angular momentum transport via the MHD turbulence, is strongly affected by the non-idea MHD effects. Thus, it is neces-

sary to study the non-idea MHD effects on the MRI before further investigating the properties of the magnetized circumplanetary disks.

We find that when $M_p \lesssim 33M_\oplus$, viscosity can disrupt the spiral structure around a protoplanet considerably and make the gas in the disk smoothly distributed, which makes the torques exerted on the protoplanet weaker. Thus, viscosity can make the migration speed of a protoplanet lower. This is helpful to solve the problem that a protoplanet quickly migrates to the vicinity of the central star before becoming a gas giant planet.

According to the core accretion theory, the formation process of a gas giant planet can be divided into three phases. (1) In phase 1, the solid core forms first, which has a mass of several Earth mass. (2) In phase 2, a spherically hydrostatic gas envelope around the solid core forms. The gas accretion rate in this phase is very low. (3) After the point when the core mass and the envelope mass become comparable, gas is accreted in a runaway fashion. The main problem of the core accretion theory is that the formation time of a gas giant planet exceeds the lifetime of the circumstellar disk. Under the assumption of spherical symmetry and gas in hydrostatic equilibrium, previous works found that the time needed to complete phase 2 is comparable or exceeding the lifetime of the circumstellar disk (e.g. Pollack et al. 1996). The reason for the longtime evolution in phase 2 is that they assume spherical accretion. The gravitational energy released in the accretion process can not easily escape from the system, the thermal pressure can support the envelope against the gravity of the core, which decreases the accretion rate in phase 2 significantly. Lin (Lin 2006) proposed that if a circumplanetary disk (instead of a spherically hydrostatic envelope) exists around a several Earth mass protoplanet, the evolution time of phase 2 may be decreased significantly. This is because in the disk accretion case, the gravitational energy released in the accretion process can easily escape from the surface of the circumplanetary disk. However, our simulation found that when the protoplanet is small (several Earth mass), the size of the circumplanetary disk is just $\sim 27\%$ of the Hill radius, R_H , when viscosity is included (see Fig.4). Thus, even though the existence of a circumplanetary disk can make the formation time of a gas giant planet smaller, we expect that the effect is not important because the size of the disk is small enough compared to the Hill radius.

Satellites may form in the circumplanetary disk. Regular satellites around a gas giant planet are considered to form according to a scenario similar to the formation of Earth-like planets in our Solar system. The protosatellite forms by the accumulation through mutual collision of the satellitesimals that form after the dust grains sink towards the equatorial plane of the circumplanetary disk (e.g. Stevenson, Harris & Lunine 1986). After including viscosity, the density of the circumplanetary disk increases, which should be helpful for the formation of satellitesimals by the accumulation of dust grains. However, the increase in density will result in the increase of opacity. It is difficult for high opacity circumplanetary disks to radiate its energy generated by gas accretion. Thus, the increase of density may result in the increase in temperature of the circumplanetary disks. Large fraction of ice is found in some of the Galilean moons around the Jupiter (Schubert, Spohn & Reynolds 1986). This means that the temperature of the circumplanetary disk should be low enough for water condensation into ice (Canup & Ward 2002). In this sense, the increase of density may make it difficult for satellite formation. In order to understand the properties of the circumplanetary disk better, we need to study the viscous circumplanetary disk with radiative transfer, which is beyond the scope of this paper.

Acknowledgements We thank Ruobing Dong and T. Tanigawa for useful discussions. We thank Hsiang-Hsu Wang for numerical supports. This work was supported in part by the Natural Science Foundation of China (grants 10833002, 10825314, 11103059, 11121062, and 11133005), the National Basic Research Program of China (973 Program 2009CB824800), and the CAS/SAFEA International Partnership Program for Creative Research Teams. The simulations were carried out at Shanghai Supercomputer Center.

References

Bai X. N., Stone J. M., 2011, *ApJ*, 736, 144

- Balbus S. A., Hawley J. F., 1991, *ApJ*, 376, 214
- Balbus S. A., Hawley J. F., 1998, *Rev. Mod. Phys.*, 70, 1
- Bate M. R., Lubow S. H., Ogilvie G. I., Miller K. A., 2003, *MNRAS*, 341, 213
- Bodenheimer P., Pollack J. B., 1986, *Icarus*, 67, 391
- Bryden G., Chen X., Lin D. N. C., Nelson R. P., Papaloizou J. C. B., 1999, *ApJ*, 514, 344
- Canup R. M., Ward W. R., 2002, *AJ*, 124, 3404
- Crida A., Baruteau C., Kley W., Masset F., 2009, *A&A*, 502, 679
- D'Angelo G., Henning T., Kley W., 2002, *A&A*, 385, 647
- D'Angelo G., Kley W., Henning T., 2003, *ApJ*, 586, 540
- Goldreich P., Lynden-Bell D., 1965, *MNRAS*, 130, 125
- Goldreich P., Tremaine S., 1979, *ApJ*, 233, 857
- Hubickyj O., Bodenheimer P., Lissauer J. J., 2005, *Icarus*, 179, 415
- Hayashi C., 1981, *Prog. Theor. Phys. Suppl.*, 70, 35
- Hayashi C., Nakazawa K., Nakagawa Y., 1985, in *Protostars and Planets II*, ed. D. C. Black & M. S. Matthews, 1100
- Ikoma M., Nakazawa K., Emori H., 2000, *ApJ*, 537, 1013
- Ikoma M., Emori H., Nakazawa K., 2001, *ApJ*, 553, 999
- Kley W., 1999, *MNRAS*, 303, 696
- Kley W., D'Angelo G., Henning T., 2001, *ApJ*, 547, 457
- Lin D. N. C., 2006, in Klahr H., Brandner W., eds, *Planet Formation*. Univ. of Cambridge Press, P. 256
- Lubow S. H., Seibert, M., Artymowicz P., 1999, *ApJ*, 526, 1001
- Machida M. N., Kokubo E., Inutsuka S., Matsumoto T., 2008, *ApJ*, 685, 1220
- Machida M. N., 2009, *MNRAS*, 392, 514
- Machida M. N., Kokubo E., Inutsuka S., Matsumoto T., 2010, *MNRAS*, 405, 1227
- Mizuno H., 1980, *Prog. Theor. Phys.*, 64, 544
- Muto T., Suzuki T. K., Inutsuka S. I., 2010, *ApJ*, 724, 448
- Muller T. W. A., Kley W., Meru F., 2012, *A&A*, 541, 123
- Papaloizou J. C. B., Nelson R. P., Snellgrove M. D., 2004, *MNRAS*, 350, 829
- Pollack J. B., Hubickyj O., Bodenheimer P., Lissauer J. J., Podolak M., Greenzweig Y., 1996, *Icarus*, 124, 62
- Quillen A. C., Trilling D. E., 1998, *ApJ*, 508, 707
- Salmeron R., Wardle M., 2005, *MNRAS*, 361, 45
- Schubert G., Spohn T., Reynolds R. T., 1986, in Burns J. A., Matthews M. S., eds, *IAU Colloq. 77: Some Background about Satellites, Thermal Histories, Compositions and Internal Structures of the Moons of the Solar System*. Univ. of Arizona Press, Tucson, P. 224
- Stone J.M., Norman M. L., 1992a, *ApJS*, 80, 753
- Stone J.M., Norman M. L., 1992b, *ApJS*, 80, 791
- Stevenson D. J., 1982, *Planet. Space Sci.*, 30, 755
- Stevenson D. J., Harris A. W., Lunine J. I., 1986, in Burns J., ed., *Satellites*. Univ. of Arizona Press, Tucson, P. 39
- Tanigawa T., Watanabe S. I., 2002, *ApJ*, 580, 506
- Tanigawa T., Ohtsuki K., Machida M., 2012, *ApJ*, 747, 47